ELSEVIER

Surface and Coatings Technology 122 (1999) 60–66

SURFACE & COATINGS TECHNOLOGY

www.elsevier.nl/locate/surfcoat

Calculation and analysis of the complex refractive index of uniform films of the As–S–Se glassy alloy deposited by thermal evaporation

E. Márquez [a,*], J.M. González-Leal [a], A.M. Bernal-Oliva [a], R. Prieto-Alcón [a], J.C. Navarro-Delgado [a], M. Vlcek [b]

[a] *Departamento de Física de la Materia Condensada, Facultad de Ciencias, Universidad de Cádiz, 11510 Puerto Real, Cádiz, Spain*
[b] *Department of General and Inorganic Chemistry. Faculty of Chemical Technology, University of Pardubice, 53210 Pardubice, Czech Republic*

Abstract

Optical reflection spectra, at normal incidence, of amorphous semiconductor thin films of chemical composition, $As_{40}S_{40}Se_{20}$, deposited by thermal evaporation, have been obtained in the 0.56–3.10 eV spectral region. The optical constants of this glassy alloy have been determined by use of an optical characterization method, which is based only on the upper and lower envelopes of the reflection spectra. Such a procedure allows accurate determination of the real and imaginary parts of the complex refractive index and the thickness of the films. Thickness measurements using a surface-profiling stylus have been carried out to cross-check the results obtained by the envelope method. The dispersion of the refractive index has been analyzed according to a new model recently proposed by Solomon. This optical dispersion model takes into consideration the width of the valence and the conduction bands, introducing a correction to the model that is based on the single oscillator. Finally, the optical-absorption edge of the *a*-$As_{40}S_{40}Se_{20}$ thin films is described in terms of the non-direct transition model proposed by Tauc, in the strong-absorption region, and in the medium-absorption region, according to Urbach's rule. © 1999 Elsevier Science S.A. All rights reserved.

1. Introduction

Optical properties of chalcogenide glasses, such as excellent transmittance in the infra-red region, continuous shift of the optical-absorption edge, and values of refractive index ranging between around 2.0 and 3.5, as well as a very strong correlation between the former properties and the corresponding chemical composition, explain the significant interest in these amorphous materials for manufacture of filters, anti-reflection coatings and, in general, a wide range of optical devices [1–3]. Furthermore, the broad range of photo-induced effects that the chalcogenide glasses exhibit [4,5], generally accompanied by large changes in the optical constants [6,7] and, particularly, shifts in the absorption edge (i.e. photo-darkening or photo-bleaching), offer the possibility of using chalcogenide glasses for high-density information storage and high-resolution display devices [8]. This clearly underlines the importance of the characterization of these glassy materials by accurate determination of their optical constants, refractive index and extinction coefficient, as well as the corresponding optical band gap.

The optical constants of thin films are usually calculated from the measured values of the film transmittance, T, reflectance, R, and thickness, d [9,10]. From the literature [11,12], it is known that the relations describing T and R are very complicated functions indeed, even for normal incidence of light. A relatively simple method for computation of the optical constants using only the optical reflection spectrum, at normal incidence, is employed in this work (mainly based on Minkov and Swanepoel's ideas of using the upper and lower envelopes of the spectrum [13–15]). These two envelopes are computer-drawn according to a useful algorithm developed by McClain et al. [16]. An important advantage of this optical procedure is that when the reflection spectrum is utilized rather than the transmission spectrum [15], a greater number of interference extrema (or equivalently, tangent points) occur, which leads to significantly reduced errors when calculating the film thickness and the refractive index [13]. In this paper, this particular method is used to accurately calculate the optical constants and the thickness of uniform thermally evaporated thin films of the ternary glassy composition, $As_{40}S_{40}Se_{20}$.

* Corresponding author. Tel.: +34-956-830966; fax: +34-956-834924.
E-mail address: emilio.marquez@uca.es (E. Márquez)

0257-8972/99/$ – see front matter © 1999 Elsevier Science S.A. All rights reserved.
PII: S0257-8972(99)00412-0

In addition, the analysis of the dispersion of the refractive index has been carried out using the well-known single-oscillator Wemple–DiDomenico model [17], and also using a new optical dispersion model recently proposed by Solomon [18]. Both allow very useful information to be obtained about the band structure of semiconductor thin films, using subgap spectroscopy. In particular, the first model allows determination of the energy difference between the 'centres of gravity', with the appropriate weighting factors, of the valence and conduction bands. However, the Solomon model goes one step further, allowing not only the aforementioned distance between the valence and conduction bands, but also the widths of these energy bands to be measured by analysis of the dispersion function of the refractive index. Finally, an analysis of the absorption coefficient has also been carried out in order to obtain the optical band gap and to determine the nature of the transitions involved.

2. Experimental

The $As_{40}S_{40}Se_{20}$ bulk glass was prepared according to the conventional melt-quenched technique. The elements were weighed and placed in a precleaned and outgassed quartz ampoule, which had been evacuated to a pressure of about 10^{-3} Pa and, then, sealed. The synthesis was performed in a rocking furnace at $\approx 715°C$ for about 6 h. Then, the ampoule was quenched in water at a temperature of $\approx 15°C$, equivalent to a cooling rate of the order of $10\ K\ s^{-1}$. Next, the thin-film samples were prepared by vacuum evaporation of the powdered melt-quenched glassy material onto clean glass substrates (microscope slides). The thermal evaporation process was performed within a coating system (Tesla Corporation, model UP-858) at a pressure of about 10^{-4} Pa. During the deposition process, the substrates were conveniently rotated by means of a very efficient planetary rotation system, thus making it possible to obtain as-deposited chalcogenide films of outstanding uniform thickness. The deposition rate was ≈ 6–$8\ nm\ s^{-1}$, measured by the dynamical weighting procedure. This deposition rate results in a film chemical composition that is very close to that of the bulk starting material. The composition of the present chalcogenide films was found to be $As_{39.8\pm0.5}S_{39.9\pm0.6}Se_{20.3\pm0.3}$, on the basis of the electron microprobe X-ray analysis (Jeol, model JSM-820). The lack of crystallinity in the films was verified by X-ray diffraction measurements (Philips, model PW-1820).

The reflection spectra were obtained by a double-beam, ratio-recording UV/Vis/NIR spectrophotometer, with automatic computer data acquisition (Perkin-Elmer, model Lambda-19), and the photon energy range analyzed was between 0.56 and 3.10 eV (or, equivalently, in the wavelength range of 2200–400 nm). The reflection measurements were carried out against a very accurately calibrated front-surface aluminium mirror coated with magnesium fluoride, which was taken as a reference. Since the absolute reflectance of the calibrated mirror is known, the relative reflectance of the thin-film sample, obtained using the spectrophotometer, can be converted to absolute reflectance. However, the reflection measurements were made in various parts of the glass films, scanning the entire sample, and a very good reproduction of the reflection spectrum was generally achieved. The spectrophotometer was set with a slit width of 1 nm. A surface-profiling stylus (Sloan, model Dektak 3030) was also used to measure the film thickness independently, and this was compared with the thickness calculated only from the optical reflection spectrum. The thickness of the *a*-$As_{40}S_{40}Se_{20}$ films studied ranged between around 0.8 and 1.4 μm. All the optical measurements reported in this paper were performed at room temperature.

3. Preliminary theoretical considerations

The inset of Fig. 1 shows the optical system under consideration, which is a homogeneous thin film with a constant thickness, d, and a complex refractive index, $n_c = n - ik$, where n is the refractive index, and k is the extinction coefficient, which in turn can be expressed in terms of the absorption coefficient α by the following

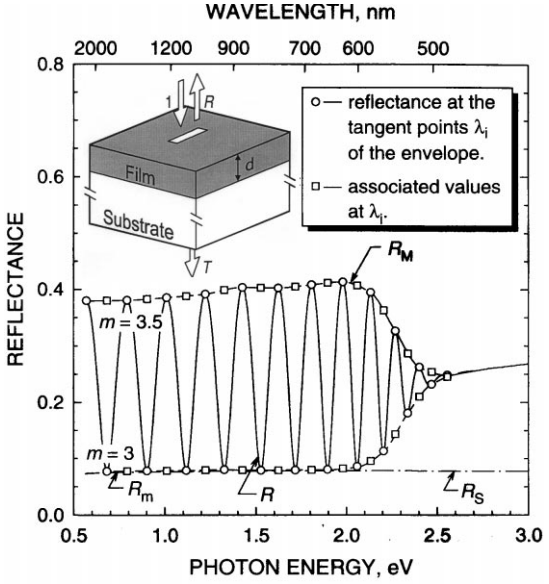

Fig. 1. Experimental optical reflection spectrum, at normal incidence, of the representative *a*-$As_{40}S_{40}Se_{20}$ thin film. The order number, m, is a half-integer for the tangent points of the higher envelope, R_M, and an integer for the tangent points of the lower envelope, R_m. R_s is the bare-substrate reflection. A sketch of the optical system under study is also shown.

equation: $k=\alpha\lambda/4\pi$ (λ, being the wavelength of the incident light). The thickness of the substrate is several orders of magnitude larger than d, and its refractive index is designated by s. Interference effects in the thin film give rise to reflectance curves similar to that displayed in Fig. 1, which corresponds to a representative $As_{40}S_{40}Se_{20}$ chalcogenide glass film. The interference fringes are used to calculate accurately the optical constants and the thickness of the As–S–Se uniform films. At a certain wavelength, λ, of the studied spectral region, the reflectance $R(\lambda; s, n, d, k)$ of the optical system mentioned earlier is a very complex function (Eq. (3) from [13]). It is known that for weakly absorbing dielectric films, when the conditions $n \gg k$ and $s \gg k$ are met in the spectral region considered, this particular equation is clearly dominated by the exponential terms in the optical absorbance, x [$=\exp(-\alpha d)$], the contribution of k in the other terms of the expression becomes negligibly small, and k can be considered to be zero [13,19]. This simplifies notably the expression for the reflectance, which becomes a function of n and x only. Expressions for the top and bottom envelopes of the reflection spectrum, R_M and R_m, respectively, are given by Eq. (5) from [13], for $k=0$ and dielectric films with $n > s \gg k$. The top envelope, R_M, lies above the spectrum, i.e. $R_M \geq R(\lambda)$, whereas the bottom envelope, R_m, lies below the spectrum, i.e. $R_m \leq R(\lambda)$. It should be pointed out that, in the present work, the refractive index of the substrate, s, is calculated independently from the reflection spectrum of the bare substrate, R_S, by the following relationship:

$$s=\frac{1+\sqrt{R_S(2-R_S)}}{1-R_S}. \quad (1)$$

4. Results and discussion

4.1. Calculation and analysis of the refractive index

First of all, it is necessary to draw the envelopes R_M and R_m, illustrated in Fig. 1. As already mentioned, these envelopes are very carefully drawn using the computer program created by McClain et al. This program enables the two envelopes of a given set of oscillatory data to be calculated accurately, based on the determination of the corresponding tangent points between the set of data and the envelopes. Due to the specific behaviour of the reflection spectra in the spectral region of medium absorption, it is not possible to use a simple parabolic interpolation when drawing the two envelopes of reflection spectra; nevertheless, such interpolation is acceptable for transmission spectra [15]. It is found that the tangent points coincide with the maxima and minima of the reflection spectrum in the transparent region, but not in the medium- and strong-absorption region. The presence of optical absorption in the film leads to smaller wavelengths for the tangent points, λ_i, with respect to the corresponding extremum points, λ_{extr} (i.e. $\lambda_i \leq \lambda_{extr}$). The effect of absorption is corrected by using the values of R and its corresponding envelopes at the tangent points, instead of the extremum points of the reflection spectrum [20].

Once the tangent points, λ_i, between the two envelopes and the reflection spectrum are known, and the refractive index of the substrate, s, is calculated from the reflection spectrum of the bare substrate, R_S, the system of two transcendental equations corresponding to Eq. (5) from [13], is solved numerically using the Newton–Raphson method. A distinct advantage of using the envelopes of the reflection spectrum, rather than only the reflection spectrum, is that the envelopes are slow-changing functions of λ, while the spectrum varies very rapidly with λ. Correspondingly, the above-mentioned system of two equations with two unknowns has only one solution for n and x. Therefore, n and x are determined for all the tangent points λ_i associated with the upper and lower envelopes, drawn by computer using McClain et al.'s algorithm, as solutions of the systems:

$$R_M(\lambda_i)-R_M(n_i, x_i)=0, \quad R_m(\lambda_i)-R_m(n_i, x_i)=0, \quad (2)$$

where $R_M(\lambda_i)$ and $R_m(\lambda_i)$ are the values of the two envelopes at the tangent point λ_i. For each tangent point, the solution of its corresponding system provides an initial approximation for the refractive index and absorbance of the thin film studied, n_i^0 and x_i^0, respectively, and these values are both listed in Table 1.

The algorithm for the derivation of the final spectral dependencies $n(\lambda)$ and $k(\lambda)$, and the film thickness of a thin layer, using exclusively the reflection spectrum, is explained in detail in Ref. [13]. The calculations are performed in the same sequence as in the method proposed by Swanepoel [15], where the transmission spectrum is used instead. In order to obtain the initial approximation for the film thickness, it is necessary to take into account the well-known equation for the interference fringes, which, due to absorption, is verified at the tangent points:

$$2nd=m\lambda, \quad (3)$$

where the order number, m, is an integer for a lower tangent point and half-integer for an upper tangent point. Moreover, if n_i and n_{i+1} are the refractive indices for two adjacent tangent points with wavelengths λ_i and λ_{i+1}, respectively, the expression for the approximate thickness associated at each tangent point is:

$$d=\frac{\lambda_i\lambda_{i+1}}{4(\lambda_i n_{i+1}-\lambda_{i+1}n_i)}. \quad (4)$$

The values of d determined by this equation are listed

Table 1
Values of λ, $\hbar\omega$, s, R_M and R_m at the tangent points, corresponding to the optical reflection spectrum of Fig. 1: calculation of the film thickness and the refractive index, based on the present envelope method

λ (nm)	$\hbar\omega$ (eV)	s	R_M	R_m	n^0	x^0	d^0 (nm)	m^0	m	d^1 (nm)	n^1
1821	0.68	1.491	0.380	0.077	2.523	0.914	–	3.13	3.0	1083	2.479
1566	0.79	1.495	0.381	0.078	2.521	0.923	1115	3.63	3.5	1087	2.487
1375	0.90	1.497	0.383	0.078	2.529	0.923	1089	4.15	4.0	1087	2.495
1228	1.01	1.497	0.385	0.078	2.544	0.917	1076	4.68	4.5	1086	2.507
1110	1.12	1.499	0.388	0.078	2.548	0.925	1114	5.18	5.0	1089	2.518
1014	1.22	1.501	0.392	0.079	2.569	0.919	1054	5.72	5.5	1086	2.530
935	1.33	1.505	0.399	0.080	2.590	0.929	1056	6.25	6.0	1083	2.545
870	1.43	1.510	0.404	0.079	2.548	1.000	1567	6.61	6.5	1109	2.566
812	1.53	1.504	0.403	0.079	2.585	0.950	985	7.19	7.0	1100	2.579
764	1.62	1.505	0.403	0.079	2.584	0.950	1254	7.64	7.5	1109	2.600
722	1.72	1.505	0.405	0.079	2.598	0.945	1157	8.13	8.0	1112	2.621
686	1.81	1.505	0.409	0.080	2.619	0.935	1140	8.62	8.5	1113	2.646
654	1.90	1.506	0.412	0.081	2.642	0.925	1123	9.12	9.0	1114	2.671
626	1.98	1.506	0.414	0.082	2.681	0.890	1029	9.67	9.5	1109	2.698
602	2.06	1.506	0.407	0.086	2.707	0.839	1168	10.2	10.0	1112	2.731
581	2.13	1.507	0.395	0.096	2.764	0.737	962	10.7	10.5	1104	2.768
562	2.21	1.507	0.363	0.113	2.780	0.596	1314	11.2	11.0	1112	2.805
546	2.27	1.507	0.327	0.144	2.823	0.416	1123	11.7	11.5	1112	2.849
530	2.34	1.507	0.287	0.181	2.857	0.233	1136	12.2	12.0	1113	2.886
516	2.40	1.504	0.263	0.210	2.890	0.112	1190	12.6	12.5	1116	2.926
502	2.47	1.503	0.254	0.232	2.945	0.046	937	13.2	13.0	1108	2.961
	$\overline{d^0} = 1130 \pm 139$ nm (12.3%); $\overline{d^1} = 1102 \pm 12$ nm (1.1%)										

as d^0 in Table 1. The average of the values of d determined by this equation, $\overline{d^0}$, is a first estimation of the film thickness. The $\overline{d^0}$ value corresponding to the representative $As_{40}S_{40}Se_{20}$ thin-film sample is 1130 ± 139 nm (12.3%). This value is used, together with n^0's, to calculate the 'order number', m^0, using Eq. (3), for the different tangent points. The accuracy of the film thickness is then very significantly increased by taking the corresponding exact integer or half-integer values of m, associated with each tangent point (see Fig. 1), and deriving a new thickness, d^1, from Eq. (3), again using the n^0 values. The values of m^0, m and d^1 are also presented in Table 1. The new values for the layer thickness do have a much smaller dispersion, and its average value is taken as the final thickness of the film. The average thickness, $\overline{d^1}$, for the representative specimen is 1102 ± 12 nm (1.1%). In addition, the film thickness determined by mechanical measurements on the same film area was 1120 ± 22 nm, in excellent agreement with the thickness obtained by the optical procedure, the difference being less than 2%.

However, using the exact values of m and the $\overline{d^1}$ value, Eq. (3) is solved for n at each λ_i and, thus, the final values of the refractive index, n^1's, are calculated (these new values are also given in Table 1). These n^1's can be fitted to an appropriate function, such as the Wemple–DiDomenico dispersion relationship [17]. This model describes the dielectric response for transitions below the optical gap, E_g^{opt}, reducing the complex valence- and conduction-band system to a two-level system, with the simple one-oscillator formula:

$$n^2(\hbar\omega) - 1 = (n_0^2 - 1)\,\frac{E_M^2}{E_M^2 - (\hbar\omega)^2}, \qquad (5)$$

where $\hbar = h/2\pi$ (h is Planck's constant), ω is the frequency, $n(\hbar\omega)$ is the value of the refractive index at the photon energy $\hbar\omega$ and n_0 is the static refractive index (i.e. extrapolated to photon energy zero). The quantity E_M is the average energy gap parameter, which is likened in this particular model to the energy difference between the two levels of a one-oscillator system (see Fig. 2). Plotting $(n^2-1)^{-1}$ against $(\hbar\omega)^2$ and fitting a straight line enables the determination of n_0 and E_M, directly from the slope and the intercept on the vertical axis. The straight line equation corresponding to the least-squares fit is, $(n^2-1)^{-1} = 0.199 - 0.0096\,(\hbar\omega)^2$, with a correlation coefficient of 0.9994 (see Fig. 2). The values found for the dispersion parameters corresponding to Eq. (5), n_0 and E_M, are: $n_0 = 2.454 \pm 0.001$ and $E_M = 4.55 \pm 0.03$ eV. These values are consistent with those reported in Ref. [21] for $As_{40}S_{60}$ and $As_{40}Se_{60}$ binary chalcogenide glass films, and in Ref. [22] for $As_{40}S_{60-x}Se_x$ ternary bulk glasses, as we have discussed in a previous study [23]. The experimental variation of the refractive index with the photon energy, $n(\hbar\omega)$, is shown in Fig. 3, along with the optical dispersion curve corresponding to Eq. (5). However, from both Figs. 2 and 3, it can be seen that the experimental variation in the refractive index clearly departs from that given by

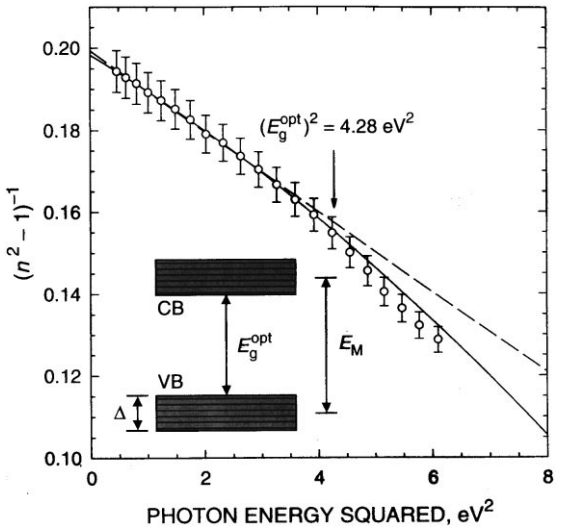

Fig. 2. Plot of the refractive-index factor, $(n^2-1)^{-1}$, versus the photon energy squared, $(\hbar\omega)^2$, to fit the experimental values of the refractive index to the two optical dispersion relationships mentioned in the text. The dashed and solid lines correspond to the Wemple–DiDomenico and Solomon models, respectively. Also, a simplified picture corresponding to the band structure of a semiconductor, is shown. This is characterized by three parameters: the optical gap, E_g^{opt}, the average gap, E_M, and the bandwidth, Δ.

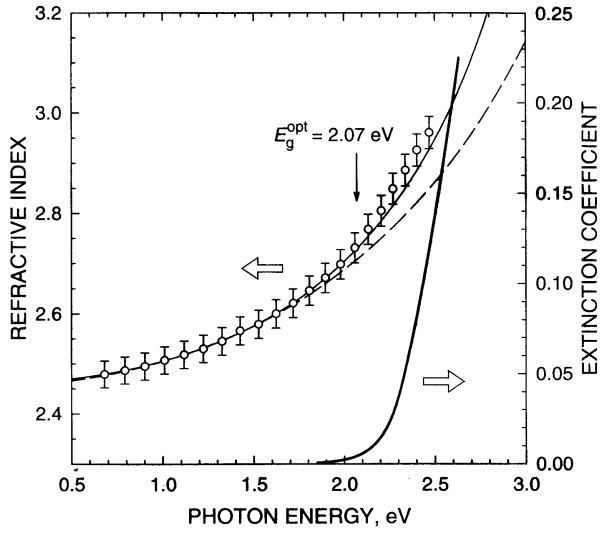

Fig. 3. Variation of the refractive index, n, with the photon energy for the representative a-$As_{40}S_{40}Se_{20}$ film. The variation of n is fairly well verified by the one-oscillator formula (dashed line), except around the optical gap, E_g^{opt} (vertical arrow), and beyond. In this region, the Solomon dispersion relationship shows a better fit (solid line). The thicker line corresponds to the plot of the extinction coefficient, k, as a function of the photon energy.

Eq. (5), when the photon energy approaches the optical-gap value. In this concrete case, the one-oscillator approximation fails, and the width of the bands induces some divergence, due to the denominator term in Eq. (5); one would expect a variation in n faster than that given by the one-oscillator formula, which is, indeed, what is observed in Fig. 2. Nevertheless, for a photon energy well below the optical gap, the Wemple–DiDomenico optical dispersion relationship provides an excellent experimental fit to the measured refractive index.

A new optical dispersion model has recently been proposed by Solomon [18], which, very importantly, takes into account the effect of the width of the bands, when the photon energy is not infinitely small compared with the optical gap, by the following relationship:

$$n^2(\hbar\omega)-1=(n_0^2-1)\,\frac{1}{1-(\hbar\omega)^2/E_c^2-\beta((\hbar\omega)^4/E_c^4)}, \qquad (6)$$

with

$$E_c^2=E_M^2-\Delta^2 \text{ and } \beta=\frac{4}{3}\frac{\Delta^2}{E_c^2}.$$

Considering square-shaped bands, i.e. a constant density of states from the bottom to the top of each energy band, the value of Δ will then be a quantity measuring the 'effective width' of the bands. It is obvious that, when the width, Δ, of the bands is considered to be zero, Eq. (6) reduces to the one-oscillator formula.

However, it is important to note that this new model assumes that the widths of the valence and conduction bands are equal, which would be verified, for instance, in the case of silicon-based amorphous semiconductors [18,24]. However, in the case of chalcogenide glassy semiconductors, the band structure is slightly more complex, although for stoichiometric compositions of the type As_2C_3, where C represents a chalcogen element, assuming that there are only heteropolar chemical bonds, the graph of the density of electronic states shows some degree of symmetry. This degree of symmetry is only slightly broken by a close distribution of the states, corresponding to the lone-pair electrons associated with the p-orbitals of the chalcogen element [25]. Thus, for the ternary chalcogenide alloy studied in this work, considering that its 'stoichiometric composition' is $As_2(S_{2/3}Se_{1/3})_3$, and considering the presence of basically heteropolar bonds, it seems reasonable to apply the novel Solomon optical dispersion model to the experimental values of the refractive index that have been previously determined. Of course, the values for the parameters related to the structure of the bands that are presently derived, although significant, will only be reasonably approximate.

Fig. 2 also shows the fit of the experimental values of the refractive index to the Solomon relationship. The parabola equation corresponding to the least-squares fit is, $(n^2-1)^{-1}=0.198-0.0082(\hbar\omega)^2-0.00043(\hbar\omega)^4$, with a correlation coefficient of 0.9998. A better agreement between the experimental values and this new dispersion relationship is found, particularly when the photon

energy approaches the value of the optical gap. The values obtained for the parameters related to this dispersion model have been: $n_0 = 2.459 \pm 0.001$, $E_M = 6.83 \pm 0.46$ eV and $\Delta = 4.75 \pm 0.46$ eV. Comparing these new values with those obtained previously, from the Wemple–DiDomenico relationship, it should be mentioned that, the value of n_0 remains almost the same, whereas the value of E_M clearly increases ($\approx 50\%$). It should also be pointed out that similar changes were found by Solomon in *a*-Si:H thin films [18]. In addition, from the schematic band structure displayed in the inset of Fig. 2, it is concluded that the three parameters E_g^{opt}, E_M and Δ are not independent: $E_M = E_g^{opt} + \Delta$. Therefore, from the aforementioned values of E_M and Δ, the value of the optical gap can be estimated: $E_g^{opt} = 2.08$ eV. Finally, Fig. 3 also shows the new optical dispersion curve, drawn from the Solomon dispersion parameters calculated previously.

4.2. Derivation and analysis of the optical-absorption edge

Extrapolating either of the two above optical dispersion models towards the absorption region, the absorbance, x, can be derived by numerically solving either of the two expressions for the envelopes corresponding to Eq. (5) from Ref. [13] (it is possible to solve both equations independently for x, thereby obtaining two different values). Furthermore, since x and d are already known, the absorption and extinction coefficients can be determined. The results obtained from the envelope R_M are found to be superior, and this can be attributed to the fact that R_m is almost independent of n and k in the region of weak absorption where $x \approx 1$. Moreover, in the region of transparency, where $x = 1$, $R_m = R_s$, and it can be seen from Eq. (1) that R_m is independent of n and k. Therefore, the values of the absorption coefficient, α, and the extinction coefficient, k, have been derived using the upper envelope of the reflection spectrum of Fig. 1. The dependence of the absorption coefficient on photon energy is displayed in Fig. 4, using a semi-logarithmic scale. Fig. 3 also shows the extinction coefficient as a function of the photon energy. It should be noted that similar results have been found using either of the two optical dispersion models under consideration.

To obtain the thin-film optical gap and to determine the nature of the optical transitions involved, the dependence of the absorption coefficient on the photon energy will now be analyzed. According to Tauc [26], it is possible to separate three distinct regions in the optical-absorption edge for amorphous semiconductors: the weak-absorption tail, which originates from defects and impurities, the exponential-edge region, which is strongly related to the structural randomness of the glassy material, and the high-absorption region, which determines

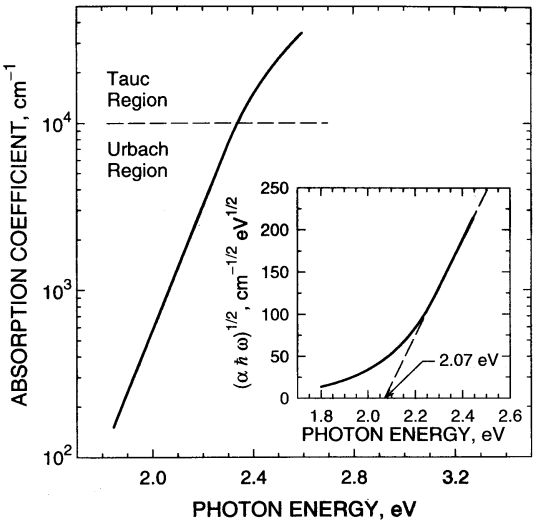

Fig. 4. Optical-absorption edge for the *a*-$As_{40}S_{40}Se_{20}$ layer, showing the Tauc and Urbach regions. The inset shows the dependence of $(\alpha\hbar\omega)^{1/2}$ on the photon energy for the determination of the optical band gap, E_g^{opt}, in terms of Tauc's law.

the optical energy gap. In the exponential-edge region (where $1\ cm^{-1} < \approx \alpha < \approx 10^4\ cm^{-1}$), the absorption coefficient is governed by the so-called Urbach relation [26,27]:

$$\alpha(\hbar\omega) = \alpha_0 \exp\left(\frac{\hbar\omega}{E_e}\right), \tag{7}$$

where E_e characterizes the slope of the exponential-edge region. Plotting the dependence of log α vs. $\hbar\omega$, as shown in Fig. 4, should give a straight line. The obtained value of E_e, the inverse of the slope, gives the width of the tails of the localized states at the band gap. The E_e value found for the representative *a*-$As_{40}S_{40}Se_{20}$ film is 104 ± 2 meV.

In the high-absorption region ($\alpha > \approx 10^4\ cm^{-1}$), involving inter-band optical transitions between valence and conduction bands, the absorption coefficient of amorphous semiconductors, is given, according to Tauc [26], by the following quadratic relation:

$$\alpha(\hbar\omega) = B\frac{(\hbar\omega - E_g^{opt})^2}{\hbar\omega}, \tag{8}$$

where B is a constant that depends on the transition probability, and E_g^{opt} is the optical energy gap. The values of E_g^{opt} and B can be readily derived from Eq. (8), by plotting $(\alpha\hbar\omega)^{1/2}$ vs. $\hbar\omega$. A very good fit between the experimental points and the straight line corresponding to the $(\alpha\hbar\omega)^{1/2}$ vs. $\hbar\omega$ plot, shown in the inset of Fig. 4, indicates that non-direct transition is the mechanism responsible for the optical absorption in the investigated *a*-$As_{40}S_{40}Se_{20}$ films. The values of the Tauc gap, E_g^{opt}, and Tauc slope, $B^{1/2}$, found for the representative thin-film sample are, 2.07 ± 0.01 eV and

$571 \pm 5\ \mathrm{cm}^{-1/2}\ \mathrm{eV}^{-1/2}$, respectively. Also, these results are consistent with those reported in Ref. [21], which have been analyzed in detail in our previous paper [23]. It should be pointed out that the value of E_g^{opt}, 2.07 eV, obtained from the analysis of the optical-absorption edge, agrees well with that previously determined from the analysis of the dispersion of the refractive index, in terms of the Solomon model: 2.08 eV. This fact suggests that, it is certainly reasonable to apply this useful dispersion model to describe the dielectric response of the present amorphous $As_{40}S_{40}Se_{20}$ films below the Tauc gap.

5. Concluding remarks

Optical characterization of chalcogenide amorphous semiconductor thin films, with uniform thickness, and chemical composition, $As_{40}S_{40}Se_{20}$, has been carried out using a method based only on the envelopes of the optical reflection spectra, measured at normal incidence. At the same time, this procedure allows accurate determination of the thickness of the films, which has been cross-checked by mechanical measurements, using a surface-profiling stylus. Moreover, the dispersion of the refractive index has been studied, in the subgap region, in terms of a novel model proposed recently by Solomon, which clearly improves the single-oscillator Wemple–DiDomenico framework, mainly when the photon energy approaches the optical-gap value (although the single-oscillator formula provides a fairly good experimental fit for photon energies well below E_g^{opt}). The results obtained using the Solomon relationship suggest that it is reasonable to make use of this refractive index dispersion model in order to describe the dielectric response of amorphous $As_{40}S_{40}Se_{20}$ layers below the optical gap. Finally, the optical-absorption edge is appropriately fitted to the non-direct transition model proposed by Tauc, in the strong-absorption region, and to the Urbach relation, in the medium-absorption region.

Acknowledgements

The authors are grateful to Dr D.A. Minkov (Research Institute for Fracture Technology, Tohoku University, Sendai, Japan) and to Prof. R. Swanepoel (University of Rand Afrikaans, South Africa) for some very fruitful discussions. This work was supported by CICYT (Spain) under MAT98-0791 project.

References

[1] J.A. Savage, Infrared Optical Materials and their Antireflection Coatings, Adam Hilger, Bristol, UK, 1985.
[2] S.R. Elliott, Physics of Amorphous Materials, Longman, New York, 1990.
[3] Z. Cimpl, F. Kosek, Phys. Stat. Sol. (a) 93 (1986) K55.
[4] E. Márquez, R. Jiménez-Garay, A. Zakery, P.J.S. Ewen, A.E. Owen, Phil. Mag. B 63 (1991) 1169.
[5] E. Márquez, C. Corrales, J.B. Ramírez-Malo, J. Reyes, J. Fernández-Peña, P. Villares, R. Jiménez-Garay, Mater. Lett. 20 (1994) 183.
[6] E. Márquez, J.B. Ramírez-Malo, J. Fernández-Peña, P. Villares, R. Jiménez-Garay, P.J.S. Ewen, A.E. Owen, J. Non-Cryst. Solids 164 (1993) 166–1223.
[7] E. Márquez, J.B. Ramírez-Malo, J. Fernández-Peña, R. Jiménez-Garay, P.J.S. Ewen, A.E. Owen, Opt. Mater. 2 (1993) 143.
[8] S.R. Ovshinisky, H. Fritzsche, IEEE Trans. Electron. 20 (1973) 91.
[9] J. Szcyrbrowski, K. Schmalzbauer, N. Hoffmann, Thin Solid Films 130 (1985) 57.
[10] L. Vriens, W. Rippens, Appl. Opt. 22 (1983) 4105.
[11] D.Y. Lou, Appl. Opt. 21 (1982) 1602.
[12] S.G. Tomlin, J. Phys. D: Appl. Phys. 5 (1972) 847.
[13] D.A. Minkov, J. Phys. D: Appl. Phys. 22 (1989) 1157.
[14] J. Ruíz-Pérez, E. Márquez, D. Minkov, J. Reyes, J.B. Ramírez-Malo, P. Villares, R. Jiménez-Garay, Phys. Scripta 56 (1996) 76.
[15] R. Swanepoel, J. Phys. E: Sci. Instrum. 16 (1983) 1214.
[16] M. McClain, A. Feldman, D. Kahaner, X. Ying, Comput. Phys. 5 (1991) 45.
[17] S.H. Wemple, M. DiDomenico, Phys. Rev. B 3 (1971) 1338.
[18] I. Solomon, Phil. Mag. B 76 (1997) 273.
[19] R. Swanepoel, S. Afr. J. Phys. 12 (1989) 148.
[20] R. Swanepoel, J. Phys. E.: Sci. Instrum. 17 (1984) 896.
[21] J.B. Ramírez-Malo, E. Márquez, C. Corrales, P. Villares, R. Jiménez-Garay, Mater. Sci. Eng. B 25 (1994) 53.
[22] J.S. Sanghera, V.Q. Nguyen, I.D. Aggarwal, J. Am. Ceram. Soc. 79 (1996) 1324.
[23] E. Márquez, J.M. González-Leal, R. Prieto-Alcón, M. Vlcek, A. Stronski, T. Wagner, D.A. Minkov, Appl. Phys. A 67 (1998) 371.
[24] I. Solomon, M.P. Schmidt, C. Sénémaud, M. Driss Khodja, Phys. Rev. B 38 (1988) 13 263.
[25] S.R. Elliott, Chalcogenide glasses, in: J. Zarzycki (Ed.), Glasses and Amorphous Materials, VCH, Weinheim, Germany, 1991, p. 420.
[26] J. Tauc, in: J. Tauc (Ed.), Amorphous and Liquid Semiconductors, Plenum, New York, 1974.
[27] F. Urbach, Phys. Rev. B 92 (1953) 1324.